

Atmospheric studies from the Mars Science Laboratory Entry, Descent and Landing atmospheric structure reconstruction

C. Holstein-Rathlou¹ (rathlou@bu.edu), A. Maue¹, P. Withers^{1,2}

¹Center for Space Physics, Boston University, 725 Commonwealth Ave., Boston, MA 02215, USA

²Astronomy Department, Boston University, 725 Commonwealth Ave., Boston, MA 02215, USA

Abstract

The Mars Science Laboratory (MSL) entered the martian atmosphere on Aug. 6, 2012 landing in Gale crater (4.6°S, 137.4°E) in the local mid-afternoon. Aerodynamic accelerations were measured during descent and atmospheric density, pressure and temperature profiles have been calculated from this data. Using an averaging technique developed for the NASA Phoenix Mars mission, the profiles are extended to 134.1 km, twice that of the engineering reconstruction. Large-scale temperature oscillations in the MSL temperature profile are suggestive of thermal tides. Comparing the MSL temperature profile with measured Mars Climate Sounder temperature profiles and Mars Climate Database model output highlights the presence of diurnal tides. Derived vertical wavelengths for the diurnal migrating tide are larger than predicted from idealized tidal theory, indicating an added presence of nonmigrating diurnal tides. Sub-CO₂ condensation mesospheric temperatures, very similar to the Pathfinder temperature profile, allude to the possibility of CO₂ clouds. This is however not supported by recent observations and models.

1. Introduction

The Curiosity rover successfully landed on Mars on August 6, 2012 at 05:18 UTC. Landing occurred on $L_s = 150.7$, MY 31 in the local afternoon (15:03 Local Mean Solar Time (LMST), 15:36 Local True Solar Time (LTST)) at a radius of 3391.13 km for the landing site in Gale Crater (4.6°S, 137.4°E) (Way et al. 2013, Karlgaard et al. 2014, Kornfeld et al. 2014).

Data from the Entry, Descent, and Landing (EDL) of the Curiosity rover, the centerpiece of the Mars Science Laboratory (MSL) mission, have been used to obtain a profile of martian atmospheric density, pressure, and temperature from 134.1 km to 12.1 km above the surface with excellent sub-km vertical resolution.

The thermal structure of the martian atmosphere is sensitive to radiative forcing from suspended dust and to diabatic heating associated with atmospheric dynamics (Zurek et al. 1992). It is also perturbed by a wide variety of waves and tides. Although a single profile of atmospheric temperature seems trivial by comparison to the vast number of Mars Global Surveyor Thermal Emission Spectrometer and Mars Reconnaissance Orbiter (MRO) Mars Climate Sounder (MCS) profiles, the unsurpassed vertical range and resolution of entry profiles continues to make them scientifically valuable at Mars. Their "whole atmosphere sampling" of thermal structure, their surface-to-thermosphere sampling of atmospheric tides, and their ability to characterize small-scale gravity waves are all useful contributions to Mars science.

Section 2 describes how an atmospheric profile was obtained from entry data, Section 3 reports the findings of scientific analysis of that atmospheric profile, and Section 4 presents the conclusions of this work.

2. Trajectory and atmospheric structure reconstruction

MSL's entry into the atmosphere of Mars was unprecedented in many ways - largest entry mass, largest aeroshell, smallest landing ellipse, and largest lift-to-drag ratio (Dyakonov et al. 2007). Consequently, its entry system is distinctly new, rather than a simple scaling-up from the designs of past landers. During its hypersonic entry phase, the MSL entry vehicle flew at a non-zero angle of attack and had a much larger lift-to-drag ratio than any lander since Viking. Pathfinder, Spirit, Opportunity, and Phoenix all flew at near-zero angles of attack with negligible lift (Dyakonov et al. 2007, Karlgaard et al. 2014). For MSL, the direction of its lift vector was not fixed. Instead, it was actively adjusted during entry by a reaction control system in order to achieve the desired trajectory (Karlgaard et al. 2014). As a result, MSL was the first Mars lander since Viking to experience a substantial period of near-horizontal flight towards the end of its hypersonic entry phase.

Trajectory reconstruction

The MSL spacecraft carried an inertial measurement unit (IMU) that measured the 3-axis linear acceleration and 3-axis angular velocity at 200 Hz throughout the entire period of atmospheric flight (popularly known as the seven minutes of terror). Integrating these measurements forward in time from

an initial entry state at the top of the atmosphere yields a time series of spacecraft position and velocity. This task was performed by the project engineers and the reconstructed trajectory is reported and discussed in Karlgaard et al. (2014) and Dutta et al. (2014). This reconstructed trajectory, which is available as a SPICE kernel (http://naif.jpl.nasa.gov/pub/naif/MSL/kernels/spk/msl_edl_v01.bsp), is shown in Figure 1. Note that all heights in this paper should be interpreted as radial distance above the landing site, whose radial distance from the center of mass of Mars is 3391.1 km (Dutta et al. 2013). Note also that all times in this paper are referenced to the time when data was first collected at Spacecraft Clock Time 397501174.997338 s (Dutta et al. 2013, Karlgaard et al. 2014). With these conventions, atmospheric entry (defined as a radial distance of 3522.2 km) occurred at a time of 540 s and a height of 131.1 km, whereas parachute deployment occurred at a time of 799 s and a height of 12.1 km. The period of horizontal flight at about 18.4 km height, between 640 s and 720 s, is a striking feature of the trajectory, during which MSL flew 105.3 km horizontally.

Information required for atmospheric reconstruction

In addition to the trajectory information, an atmospheric reconstruction requires the measured aerodynamic accelerations. To that end, JPL supplied us with time series of the 3-axis linear accelerations experienced at the spacecraft's center of mass in the Descent Stage frame, spacecraft position and velocity in the J2000 frame, and the quaternion matrix linking the J2000 and Descent Stage frames. The Descent Stage frame is a non-inertial reference frame, fixed with respect to the Curiosity rover inside the MSL entry vehicle (<http://naif.jpl.nasa.gov/pub/naif/MSL/kernels/fk/msl.tf>). These 200 Hz acceleration data were used in the work reported here.

The final reconstruction results are most useful in a Mars-centric spherical coordinate system rotating with the planet, as per previous reconstruction efforts (Magaelhães et al. 1999, Withers and Smith 2006, Withers and Catling 2010). Accordingly, we calculated time series of latitude, longitude and radial distance from the center of mass of Mars from the JPL supplied J2000 trajectory using SPICE routines and kernels.

The atmospheric reconstruction requires knowledge of two additional quantities which can be calculated from the available information: the speed of the spacecraft relative to the atmosphere (v_{rel}) and the (total) angle of attack (α). By assuming that the atmosphere of the planet is rotating with the same angular velocity as the interior of the planet, v_{rel} is calculated by subtracting the rotational speed of the planet at the appropriate latitude and radial distance from the spacecraft velocity relative to the center of mass of the planet. The total angle of attack is simply the angle between the vector v_{rel} and the spacecraft symmetry axis, which is fixed in the Descent Stage frame.

Enhanced aerodynamic accelerations

The delivered aerodynamic accelerations are not optimal for atmospheric reconstruction. The most important component is the axial acceleration, which is shown in Figure 2. Instrument digitization and noise render the measured accelerations unusable for reconstruction prior to 570 s, equivalent to a height of 85.1 km. In order to maximize the scientific value of MSL's atmospheric profile, we average the

measured axial acceleration using a technique developed by Withers (2013). The averaged acceleration is also shown in Figure 2. Useful accelerations now extend to 538 s (134.1 km). The averaging process inevitably worsens the temporal and spatial resolution of the dataset. However, since the sampling rate is 200 Hz and the spacecraft height only decrease by 8.18 m in 1/200 second, this is acceptable. The vertical resolution is shown in Figure 3 as a function of height. At time 660-685 s the raw axial accelerations contain considerable noise due to structural vibrations that occurred during bank reversals and heading alignment of the spacecraft during descent (Karlgaard et al. 2014). These events are evident in Figure 2, however the noise is removed during the smoothing process.

Density, pressure and temperature

With the smoothed accelerations in hand, calculating the atmospheric profiles is a simple iterative process using three main equations. This method is used only during the entry phase, when the lander is enclosed within a heat shield and spacecraft aerodynamics are relatively simple. Matters are much more complicated after parachute deployment.

Density (ρ) is calculated from the drag force equation using the smoothed axial accelerations, a :

$$\rho = -\frac{2 m_{SC} a}{C_A v_{rel}^2 A_{SC}} \quad (\text{Eq. 1})$$

where m_{SC} is the mass of the spacecraft, C_A is the axial force coefficient, v_{rel} is the speed of the spacecraft relative to the atmosphere and A_{SC} is the spacecraft area. The spacecraft area is the area of a circle of diameter 4.520 m (Schoenenberger et al. 2014). The spacecraft mass was provided to us as a function of time by JPL. The mass at atmospheric entry was 3152.5 kg, which decreased by less than 1% from 540 s to 780 s due to fuel consumption. Shortly prior to parachute deployment, at 780 s, six Entry Ballast Masses of 25 kg were ejected to eliminate lift (Schoenenberger et al. 2014, Karlgaard et al. 2014). C_A , which is on the order of 1.5 (Schoenenberger et al. 2005), varies during entry and was found from an aerodynamic database, which will be discussed shortly. To account for the poorly modelled and highly complex flowfield behind the entry capsule, C_A was adjusted using the empirically determined base pressure correction from Dyakonov et al. (2012).

Given a vertical profile of density, pressure (P) can be determined via the equation of hydrostatic equilibrium:

$$\frac{dP}{dz} = -\rho g_z \quad (\text{Eq. 2})$$

where z is height above the surface and g_z is the radial component of the gravitational acceleration as felt by the spacecraft (Withers et al. 2003), which will be a combination of the gravitational pull of Mars and the centrifugal forces. The upper boundary condition applied at $t = 538$ s (134.1 km) will be discussed in the next paragraph.

Finally, temperature (T) is calculated from the ideal gas law:

$$T = \frac{P M}{\rho k_B N_A} \quad (\text{Eq. 3})$$

where M is the mean molar mass of the martian atmosphere, k_B is the Boltzmann constant and N_A is Avogadro's number. The mean molar mass of 43.41 g/mol was calculated using the reference Mars atmosphere from the CRC Handbook. There are multiple ways to fix the upper boundary condition for pressure in the equation of hydrostatic equilibrium. Here we specify it via temperature and the ideal gas law, by assuming a temperature at the upper boundary of $T = 150$ K (Nier and McElroy 1977, Withers 2006, Forget et al. 2009).

To begin the atmospheric reconstruction, we assume $C_A = 2$ and find the corresponding ρ , P and T profiles. From these, we calculate the Mach (Ma) and Knudsen (Kn) numbers along the trajectory (Withers et al. 2003) using the molecular diameter of CO_2 of 4.53×10^{-10} m (CRC Handbook) and the specific heat ratio of CO_2 of 1.4, as calculated for a linear, diatomic molecule (Atkins and de Paula 2006). Given Ma , Kn and α , an improved value of C_A can be found from MSL's aerodynamic database (Dyakonov et al. 2012, Schoenenberger et al. 2005) and the process is iterated until acceptable convergence is reached.

Challenges of horizontal flight

Finding pressure and temperature from density requires a vertical density profile. This is satisfied at high altitudes, but not during the period of horizontal flight. This is a consequence of the novel entry system employed by the MSL spacecraft and is a complication that was not encountered during atmospheric reconstructions for Pathfinder, Spirit, Opportunity, or Phoenix. Nevertheless, density may be determined via the drag force equation even during horizontal flight.

The project was aware of this issue during the design phase of the mission. Due to an engineering requirement to better understand the performance of the entry vehicle during atmospheric flight, the MSL EDL Instrumentation (MEDLI), an engineering investigation able to resolve this issue, was flown (Karlgaard et al. 2014, Chen et al. 2014). A MEDLI subsystem, MEADS (Mars Entry Atmospheric Data Systems) consisted of a set of seven pressure sensors embedded across the heatshield of the MSL entry vehicle. The atmospheric pressure and density could be determined from analysis of this set of dynamic pressure measurements. JPL developed an engineering representation of the atmospheric conditions during landing from MEADS data, IMU data, temperature profiles from MCS, and output from Mars mesoscale atmospheric models. It should be noted that the MCS profiles were not obtained at the time of landing and the output of mesoscale models is not a direct measurement of environmental conditions. The resultant engineering representation is described by Chen et al. (2014) and Karlgaard et al. (2014) and is tabulated in Chen et al. (2014).

Above 70 km, JPL considered that the atmospheric density profile could not be found from the available information. Between 18 km and 70 km, JPL found the measured aerodynamic accelerations less useful than the MEADS data and determined densities from MEADS data. Below 18 km, JPL transitioned from MEADS densities to IMU densities to model densities. MCS data at 0.5 Pa (near 60 km) were used to provide an upper boundary condition for the equation of hydrostatic equilibrium.

In order that we could also reconstruct atmospheric properties through the period of horizontal flight, JPL supplied us with a portion of this engineering representation of the atmosphere, which spans from 70.8 km ($t = 580$ s) height to parachute deployment at 12.1 km height ($t = 799$ s).

The atmospheric reconstruction reported herein uses the traditional method from 538 s (134.1 km) to 628 s (22.0 km). At later times, densities are taken from the measured aerodynamic accelerations, as before, but temperatures are taken from the engineering representation. Pressure follows from density and temperature via the ideal gas law. This transition time, which is shortly before the onset of horizontal flight, was chosen to ensure smooth continuity in the reconstructed atmospheric properties.

Results

The reconstructed atmospheric profiles are shown in Figure 4. Error envelopes were calculated for the density, pressure and temperature profiles using a run of 1000 Monte Carlo simulations in which uncertainties were introduced to the axial acceleration and axial force coefficient.

For the smoothed acceleration, uncertainty depends on the smoothing interval. For each smoothing interval the uncertainty is the standard deviation of acceleration recorded at high elevation (from $t = 450$ and 460 s) prior to the onset of detectable aerodynamic drag. The uncertainties range between 1.08×10^{-4} and 3.47×10^{-3} m/s².

An uncertainty of 5% was assigned to the axial force coefficient, which encompasses several sources of error in the determination of aerodynamic properties (Dyakonov et al. 2012). Uncertainties on the spacecraft position and velocity were neglected, since they are likely to be small in comparison to the afore-mentioned uncertainties. Uncertainties in the spacecraft mass were also neglected since entry mass and major mass losses during entry due to balance mass ejections are well known. Errors in mass due to un-modeled fuel consumption are small, less than 1%. Uncertainties in spacecraft area are absorbed into the axial force coefficient.

The temperature profile shown in Figure 4 covers twice the altitude range of the engineering temperature profile (Chen et al. 2014). This main factor responsible for this impressive doubling is use of the averaging process of Withers (2013).

3. Analysis of results

The results of the reconstruction are atmospheric profiles for density, pressure and temperature as functions of height above the landed surface (Figure 4). Density and pressure both display a near-exponential behavior for the duration of the descent, with a small 'kink' at 14.5 km height ($t = 780$ s) due to ejection of the Entry Ballast Masses which changed the total angle of attack to zero degrees to eliminate spacecraft lift (Karlgaard et al. 2014).

The most striking feature of MSL's temperature profile (Figure 5) is the deep mesopause minimum at 81.1 km height (5.36×10^{-2} Pa) where the temperature dips to 99.9 ± 0.2 K. This is colder than the CO₂ condensation temperature of 103 K for this pressure level (Magalhães et al. 1999). Directly above the

mesopause lies the thermosphere, which here is isothermal at $T = 130.0 \pm 1.4$ K between 1.14×10^{-2} Pa (90.5 km) and 1.89×10^{-3} Pa (103.2 km), a range of 1.8 scale heights. Below the mesopause, the temperature generally increases with increasing pressure. However, temperature oscillations are superimposed on this general trend.

Comparison to observations and simulations

The MSL temperature profile can be compared to atmospheric temperature profiles acquired by MCS. Unfortunately, MCS did not acquire any profiles near the landing site near the time of landing, so a direct comparison is not possible. However, comparison to a zonally-averaged set of MCS profiles is possible. Figure 5 includes the average of 49 MCS profiles acquired between $2.1 - 7.1^\circ$ S at $15.0 - 16.0$ LTST from $L_s = 145.9$ to 150.7 (Jul. 27 – Aug. 6, 2012). This time span is not centered on the time of landing because MCS ceased scientific operations from the day of landing until Sep. 9, about 1 month after landing, in order for MRO to focus on operational support for the Curiosity rover.

The MSL temperature profile can also be compared to the predicted profile from the Mars Climate Database (MCD v. 5.1), a general circulation model for Mars (Millour et al. 2014). The profile was acquired for the time and position of MSL landing under the climatological solar EUV average scenario for 70 evenly spaced pressures between 6×10^2 Pa and 1×10^{-5} Pa.

The MCD profile agrees reasonably well with the MSL profile below 60 km (2 Pa), and the average MCS profile does so below 70 km (0.3 Pa). However, neither of them reproduces the cold mesopause temperature minimum observed by MSL, with both being approximately 35 K warmer at this pressure level. Indeed, the MCD profile places the mesopause significantly higher in the atmosphere at 3.79×10^{-4} Pa (114.1 km) and the average MCS profile shows a temperature maximum near MSL's mesopause pressure level. Moreover, the MCD profile does not show any hint of the broad isothermal structure observed by MSL. One possible explanation for these differences at high altitude is that the MSL profile is strongly influenced by features that are transient in nature.

Thermal tides

The large-scale temperature oscillations visible in the MSL temperature profile are suggestive of thermal tides. Thermal tides are global-scale oscillations in atmospheric properties (density, pressure, temperature, winds) whose periods are integer fractions of the martian day, or sol (Chapman and Lindzen 1970). They are an important aspect of the dynamics of the atmosphere of Mars (Zurek 1976, 1986; Leovy and Zurek 1977, Leovy 1981, Zurek and Leovy 1981, Tillman 1988, Wilson and Hamilton 1996, Bridger and Murphy 1998, Keating et al. 1998, Banfield et al. 2000, 2003; Wilson 2002, Forbes et al. 2002, 2004; Withers et al. 2003, 2011; Forbes 2004, Moulden and Forbes 2008, 2010, 2011, 2014; Lee et al. 2009, Sato et al. 2011, Guzewich et al. 2012, 2014; Kleinbohl et al. 2013). At Mars, they are a particularly significant aspect of the climate system due to the low thermal inertia of Mars's atmosphere, which causes strong day-night temperature variations (Zurek et al. 1992). These variations become thermal tides. Two of most familiar effects of thermal tides are regular daily variations in

surface pressure with local solar time (Zurek et al. 1992, Haberle et al. 2014) and oscillations with altitude in vertical temperature profiles (Lee et al. 2009).

To test the hypothesis that the observed oscillations in temperature with altitude are caused by thermal tides, we compare the observed profile (smoothed over 0.5 scale heights to remove small scale oscillations) to a 3 scale height smoothed version of the profile, as shown in Figure 6a. In theory, the observed profile should be compared to a diurnal mean profile. Since this is not available, we use the profile smoothed over three scale heights (three orders of magnitude of pressure) to simulate this background temperature state. The temperature difference between the observed and smoothed profile in Figure 6b have maxima at 1.48 Pa and 2.83×10^{-3} Pa and minima at 12.63 Pa and 5.86×10^{-2} Pa, giving vertical wavelengths of 5.4 to 6.3 scale heights. The wave-like structure disappears at higher altitudes (above 5×10^{-3} Pa), presumably due to dissipation in the thermosphere.

These oscillations in the observed MSL temperature profile can be compared to those present in MCS observations and MCD output. Smoothed background profiles are obtained in a similar manner to MSL, as described above. Figure 6a and 6b shows that temperature oscillations are present in all three of these datasets, but the vertical structures are quite different.

In order to interpret these oscillations in the context of tidal theory, the best approach would be to compare observed temperatures against diurnal mean temperatures. However, diurnal mean temperatures are not available for the MSL entry profile. In the limit that atmospheric oscillations are dominated by diurnal and semidiurnal modes, the difference between a daytime observation and the diurnal mean can be approximated by a day-night difference. A day-night difference can be determined for the MCS and MCD profiles, but not for the MSL profile. MCS nighttime profiles were acquired under similar conditions as for the daytime profiles described earlier, restricted to a time span of 03-04 LTST, yielding 210 profiles. A nighttime MCD temperature profile was acquired for 03:36 LTST (nighttime) under the same conditions as described previously. The MCS and MCD profiles are shown in Figure 6c and the day-night differences are shown in Figure 6d. These substantial temperature differences indicate that the temperature oscillations are predominantly diurnal, not semidiurnal, in nature. The pressure levels of the maxima and minima in the MCS and MCD temperature oscillations are the same in Figure 6b and 6d. Therefore we conclude that the pressure levels of maxima and minima in the MSL temperature oscillations in Figure 6b are representative of the otherwise unobtainable day-night difference.

Idealized tidal theory provides a prediction for the vertical wavelength of tidal modes that can be compared against the observations.

$$\lambda_z = \frac{2\pi H}{(\Gamma H^2 / T h_n^{-1/4})^{1/2}} \quad (\text{Eq. 4})$$

Here H is the pressure scale height, Γ is the static stability calculated as $(dT/dz + g/c_p)$ where c_p is the specific heat capacity, T is temperature and h_n is equivalent depth of the tidal mode, which is 0.485 km for the diurnal migrating tide and 5.52 km for the semidiurnal migrating tide (Chapman and Lindzen 1970, Zurek et al. 1980, Magalhães et al. 1999). Vertical wavelengths can be calculated using a

background temperature, in this case the 3 scale height averaged MSL temperature profile. As seen in Figure 7, the typical predicted vertical wavelength is 2 scale heights for the diurnal migrating tide and 10 scale heights for the semidiurnal migrating tide. By contrast, the observed vertical wavelength in the MSL entry profile is approximately 6 scale heights. The vertical wavelength of the oscillations in the MSL temperature profile is not consistent with either a pure diurnal migrating tide or a pure semidiurnal migrating tide, however the MCS and MCD data suggest that the observed oscillations are a diurnal phenomenon.

A plausible scenario is that the diurnal migrating tide is accompanied by at least one diurnal nonmigrating tidal mode. Appreciable zonal variations, which cannot be caused by migrating tidal modes, with a wave-3 structure are present in the MCD daytime data. As seen in Figure 8, a similar structure is present in the MCD nighttime data. Examination of MCD data at 3 hour intervals shows that this feature is an eastward travelling diurnal wave, thus indicating the presence of the Diurnal Kelvin 2 (DK2) wave. The vertical wavelength of the inferred DK2 wave in the MCD output is ~ 80 km, which is close to the predicted vertical wavelength of 90-100 km (Guzewich et al. 2012). MCS nighttime data are similar to MCD predictions, which suggest that the DK2 tidal mode is present in the equatorial atmosphere at the time of MSL EDL. Owing to very incomplete longitudinal sampling in the daytime MCS data, it is not possible to compare MCD and MCS data in the daytime. The data gaps are caused by the inability of the current MCS data processing routine to deal with opaque water ice clouds (Lee et al 2009), which are prevalent in certain longitude sectors in the daytime equatorial atmosphere at this season.

Comparison to Pathfinder and possible presence of CO₂ clouds at the mesopause

Both the isothermal region in the thermosphere and the deep mesopause temperature minimum were also present in the Pathfinder entry profile. Pathfinder landed at approximately the same season as MSL ($L_s = 142^\circ$), but at night (02:58 LTST) and on the opposite side of the planet (19.1°N , 33.2°W) (Golombek et al. 1999, Haberle et al. 1999). Magalhães et al. (1999) showed that the deep temperature minimum was likely due to the diurnal migrating tide and speculated that it could be a signature of mesospheric CO₂ ice clouds. Early thoughts on CO₂ ice cloud formation from the Pathfinder data indicated that “CO₂ ice clouds should form within the temperature minima of tidal and gravity waves in the Martian mesosphere” (Clancy and Sandor 1998). At the time of the Pathfinder landing, no contemporaneous atmospheric measurements were available to test whether CO₂ ice clouds were present or not. Orbital remote sensing capabilities for observing mesospheric CO₂ ice clouds increased dramatically afterwards with the arrivals of Mars Global Surveyor in 1997, Mars Odyssey in 2001, and Mars Express in 2003, with instruments on all three orbiters having observed mesospheric CO₂ ice clouds (Clancy et al. 2007, McConnochie et al. 2010, Montmessin et al. 2007, Määttänen et al. 2010, Scholten et al. 2010).

Clouds have been observed in the tropics at the season and local time of the MSL entry, but not at the longitude of MSL entry. At this season and local time clouds are seen at longitudes of $240\text{-}300^\circ\text{E}$ and $330\text{-}30^\circ\text{E}$. Clouds have been observed above the MSL landing site at $L_s = 10\text{-}40^\circ$ (Spiga et al. 2012).

González-Galindo et al. (2011) used a Mars global circulation model (LMD-MGCM) (Forget et al. 1999, Angelats i Coll et al. 2005, González-Galindo et al. 2009) to determine the mechanisms responsible for constraining the season, local time, altitude, latitude, and longitude of the sub-condensation temperatures necessary to create the observed mesospheric CO₂ ice clouds. In their simulations they found that cold temperatures in the tropics were localized to certain longitudinal regions. They attributed this dependence on longitude to the effects of nonmigrating tides, particularly DK2. However, their mesospheric temperatures were not quite cold enough for the formation of CO₂ clouds. This obstacle was overcome by Spiga et al. (2012) who introduced gravity waves into the numerical model and were able to produce sub-condensation temperatures in these longitude regions of the tropics.

In the context of the MSL entry, none of the relevant instruments on Mars Express detected CO₂ clouds at the location and time of the MSL entry (Määttänen, private communication). Moreover, numerical simulations by Spiga et al. (2012) predict that the MSL landing site is not at the heart of a region favorable to the formation of CO₂ clouds. It is thus possible, but far from certain, that the mesospheric minimum observed by MSL is indicative of passage through a CO₂ cloud. Further numerical simulations have the potential to illuminate this question, as previous simulations of mesospheric CO₂ cloud formation have been very broad in scope.

4. Discussion and conclusions

An atmospheric temperature profile has been obtained from aerodynamic acceleration measurements obtained during the atmospheric flight of the MSL mission. This profile extends from 134.1 km to 12.1 km height above the landing site with sub-km sampling. In order for the profile to extend through a prolonged period of horizontal flight, the derived profile at heights below 22.0 km is also based on dynamic pressure measurements by the MEADS sensors. The vertical extent of this temperature profile is twice that of the comparable engineering version, which indicates the tremendous value of the averaging technique introduced by Withers et al. (2013).

Below 60-70 km, MCS temperature profiles and predictions from the MCD agree well with the MSL temperature profile. At higher altitudes, however, substantial differences appear. Large-scale temperature oscillations in the MSL temperature profile are suggestive of thermal tides. MSL, MCD and MCS temperature profiles are compared to the simulated background profiles and nighttime profiles (for the latter two) displaying the telltale signatures of a diurnal tide with a vertical wavelength of 6 scale heights. Idealized tidal theory predicts a vertical wavelength of 2 scale height, indicating that the diurnal migrating tide is accompanied by other diurnal nonmigrating tidal modes. Examination of MCD predictions and MCS data suggests the presence of the DK2 wave.

There are striking similarities between the MSL and Pathfinder atmospheric profiles, despite differences of 12 hours in local time and 180 degrees in longitude, particularly at the mesopause and in the thermosphere. The MSL atmospheric profile contains a cold mesopause of 99.9 +/- 0.2 K at 81.1km (5.36x10⁻² Pa), 3.1 K colder than the CO₂ condensation temperature at that pressure. A similar feature in the Pathfinder entry profile was conservatively attributed to the presence of mesospheric CO₂ ice

clouds. Current orbiter cloud observations and models indicate that a CO₂ cloud passing is unlikely to be the source of the MSL temperature minimum.

5. Acknowledgements

We acknowledge Anni Määttä for her time spent searching for CO₂ clouds in OMEGA and SPICAM data and Allen Chen and the MSL Council of Atmospheres for useful discussions. We acknowledge support from JPL award 1472312.

6. References

- Angelats i Coll, M., F. Forget, M.A. López-Valverde, F. González-Galindo (2005) The first Mars thermospheric general circulation model: The Martian atmosphere from the ground to 240 km, *Geophys. Res. Lett.*, 32, L04201, doi: 10.1029/2004GL021368
- Atkins, P. W. and J. de Paula (2006) *Physical Chemistry*, 8th edition, W. H. Freeman and Co., New York, ISBN: 0-7167-8759-8
- Banfield, D., B. Conrath, J.C. Pearl, M.D. Smith, P. Christensen (2000) Thermal tides and stationary waves on Mars as revealed by Mars Global Surveyor thermal emission spectrometer, *J. Geophys. Res.*, 105, pp. 9521-9537, doi: 10.1029/1999JE001161
- Banfield, D., B.J. Conrath, M.D. Smith, P.R. Christensen, R.J. Wilson (2003) Forced waves in the martian atmosphere from MGS TES nadir data, *Icarus*, 161, 319-345, doi:10.1016/S0019-1035(02)00044-1
- Bridger, A.F.C. and J.R. Murphy (1998) Mars' surface pressure tides and their behavior during global dust storms, *J. Geophys. Res.*, 103, pp. 8587-8602, doi: 10.1029/98JE00242
- Chapman, S. and R.S. Lindzen (1970) *Atmospheric tides: Thermal and gravitational*, D. Reidel, Dordrecht, Netherlands
- Chen, A., A. Cianciolo, A.R. Vasavada, C. Karlgaard, J. Barnes, B. Cantor, D. Kass, S. Rafkin, D. Tyler (2014) Reconstruction of Atmospheric Properties from Mars Science Laboratory Entry, Descent, and Landing, *J. Spacecraft and Rockets*, 51, 4, doi: 10.2514/1.A32708
- Clancy, R.T. and B.J. Sandor (1998) CO₂ ice clouds in the upper atmosphere of Mars, *Geophys. Res. Lett.*, 25, 4, pp. 489-492, doi: 10.1029/98GL00114
- Clancy, R.T., M.J. Wolff, B.A. Whitney, B.A. Cantor, M.D. Smith (2007) Mars equatorial mesospheric clouds: Global occurrence and physical properties from Mars Global Surveyor Thermal Emission Spectrometer and Mars Orbiter Camera limb observations, *J. Geophys. Res.*, 112, E04004, doi: 10.1029/2006JE002805
- CRC Handbook of Chemistry and Physics (2013) 94th Edition, CRC Press, Editor: W.M. Haynes, ISBN: 9781466571143
- Dutta, S. and R.D. Braun (2014) Statistical Entry, Descent, and Landing Performance Reconstruction of the Mars Science Laboratory, *J. Spacecraft and Rockets*, 51, No. 4, doi: 10.2514/1.A32937
- Dyakonov A.A., C.E. Glass, K.T. Edquist, M. Schoenenberger, P. Chwaloski, J. Van-Norman, W.I. Scallion, C. Tang, M.J. Wright, F.M. Cheatwood, B.R. Hollis, V.R. Lessard, N.Takashima (2007) Design Considerations for Reaction Control Systems, International Planetary Probe Workshop, June 23-29, 2007, Bordeaux, France

Dyakonov, A.A., M. Schoenenberger, J.W. Van Norman (2012) Hypersonic and Supersonic State Aerodynamics of Mars Science Laboratory Entry Vehicle, 43rd AIAA Thermophysics Conference, AIAA 2012-2999, June 25-28, 2012, New Orleans, Louisiana, USA

Forbes, J.M., A.F.C. Bridger, S.W. Bougher, M.E. Hagan, J.L. Hollingsworth, G.M. Keating, J. Murphy (2002) Nonmigrating tides in the thermosphere of Mars, *J. Geophys. Res.*, 107, 5113, doi: 10.1029/2001JE001582

Forbes, J.M. (2004) Tides in the middle and upper atmospheres of Mars and Venus, *Adv. Space Res.*, 33, pp. 125-131, doi: 10.1016/j.asr.2003.05.007

Forbes, J.M., X. Zhang, M. Angelats i Coll, G.M. Keating (2004) Nonmigrating tides in the thermosphere of Mars: a quasi-empirical description, *Adv. Space Res.*, 34, pp. 1690-1695, doi: 10.1016/j.asr.2003.09.068

Forget, F., F. Hourdin, R. Fournier, C. Hourdin, O. Talagrand, M. Collins, S.R. Lewis, P.L. Read, J.-P. Huot (1999) Improved general circulation models of the Martian atmosphere from the surface to above 80 km, *J. Geophys. Res.*, 104, E10, pp. 24,155-24,175, doi: 10.1029/1999JE001025

Forget, F., F. Montmessin, J.-L. Bertaux, F. González-Galindo, S. Lebonnois, E. Quémerais, A. Reberac, E. Dimarells, M. A. López-Valverde (2009) Density and temperatures of the upper Martian atmosphere measured by stellar occultations with Mars Express SPICAM, *J. Geophys. Res.*, 114, E01004, doi: 10.1029/2008JE003086.

Golombek, M. et al. (1999) Overview of the Mars Pathfinder Mission: Launch through landing, surface operations, data sets, and science results, *J. Geophys. Res.*, 104, E4, pp. 8523-8553, doi: 10.1029/98JE02554

González-Galindo, F., F. Forget, M. A. López-Valverde, M. Angelats i Coll, E. Millour (2009) A ground-to-exosphere Martian general circulation model: 1. Seasonal, diurnal, and solar cycle variation of thermospheric temperatures, *J. Geophys. Res.*, 114, E04001, doi: 10.1029/2008JE003246

González-Galindo, F., A. Määttänen, F. Forget, A. Spiga (2011) The martian mesosphere as revealed by CO₂ cloud observations and General Circulation Modeling, *Icarus*, 216, 10-22, doi: 10.1016/j.icarus.2011.08.006

Guzewich, S.D., E.R. Talaat, D.W. Waugh (2012) Observations of planetary waves and nonmigrating tides by the Mars Climate Sounder, *J. Geophys. Res.* 117, E03010, doi: 10.1029/2011JE003924

Guzewich, S.D., R. J. Wilson, T. H. McConnochie, A. D. Toigo, D. J. Banfield, M. D. Smith (2014) Thermal tides during the 2001 Martian global-scale dust storm, *J. Geophys. Res. Planets*, 119, pp. 506–519, doi: 10.1002/2013JE00450

- Haberle, R. et al. (1999) General circulation model simulations of the Mars Pathfinder atmospheric structure investigations/meteorology data, *J. Geophys. Res.*, 104, E4, pp. 8957-8974, doi: 10.1029/1998JE900040
- Haberle, R. M., et al. (2014), Preliminary interpretation of the REMS pressure data from the first 100 sols of the MSL mission, *J. Geophys. Res. Planets*, 119, 440–453, doi: 10.1002/2013JE004488.
- Karlgaard, C., P. Kutty, M. Schoenenberger, M.M. Munk, A. Little, C.A. Kuhl, J. Shidner (2014) Mars Science Laboratory Entry Atmospheric Data System Trajectory and Atmospheric Reconstruction, *J. Spacecraft and Rockets*, 51, 4, doi: 10.2514/1.A32770
- Keating et al. (1998) The structure of the upper atmosphere of Mars: In situ accelerometer measurements from Mars Global Surveyor, *Science*, 279, pp. 1672-1676, doi: 10.1126/science.279.5357.1672
- Kleinbohl, A., R.J. Wilson, D. Kass, J.T Schofield, D.J. McCleese (2013) The semidiurnal tide in the middle atmosphere of Mars, *Geophys. Res. Lett.*, 40, pp. 1952-1959, doi: 10.1002/grl.50497
- Kornfeld, R.P., R. Prakash, A.S. Devereaux, M.E. Greco, C.C. Harmon, D.M. Kipp (2014) Verification and Validation of the Mars Science Laboratory/Curiosity Rover Entry, Descent, and Landing System, *J. Spacecraft and Rockets*, 51, 4, doi: 10.2514/1.A32680
- Lee, C. , W.G. Lawson, M.I. Richardson, N.G. Heavens, A. Kleinböhl, D. Banfield, D.J. McCleese, R. Zurek, D. Kass, J.T. Schofield, C.B. Leovy, F.W. Taylor, A.D. Toigo (2009) Thermal tides in the Martian middle atmosphere as seen by the Mars Climate Sounder, *J. Geophys. Res.*, 114, E03005, doi: 10.1029/2008JE003285
- Leovy, C.B. (1981) Observations of Martian tides over two annual cycles, *J. Atmos. Sci.*, 38, pp. 30-39, doi: [http://dx.doi.org/10.1175/1520-0469\(1981\)038<0030:OOMTOT>2.0.CO;2](http://dx.doi.org/10.1175/1520-0469(1981)038<0030:OOMTOT>2.0.CO;2)
- Leovy, C.B. and R.W. Zurek (1979) Thermal tides and Martian dust storms – Direct evidence for coupling, *J. Geophys. Res.*, 84, pp. 2956-2968, doi: 10.1029/JB084iB06p02956
- Määttänen, A., F. Montmessin, B. Gondet, F. Scholten, H. Hoffmann, F. González-Galindo, A. Spiga, F. Forget, E. Hauber, G. Neukum, J.-P. Bibring, J.-L. Bertaux (2010) Mapping the mesospheric CO₂ clouds on Mars: MEx/OMEGA and MEx/HRSC observations and challenges for atmospheric models, *Icarus*, 209, pp. 452–469, doi:10.1016/j.icarus.2010.05.017
- Magalhães, J.A., J.T. Schofield, A. Seiff (1999) Results of the Mars Pathfinder atmospheric structure investigation, *J. Geophys. Res.*, 104, pp. 8943–8956, doi: 10.1029/1998JE900041
- McConnochie, T.H., J.F. Bell III, D. Savransky, M.J. Wolff, A.D. Toigo, H. Wang, M.I Richardson, P.R. Christensen (2010) THEMIS-VIS observations of clouds in the martian mesosphere: Altitudes, wind speeds, and decameter-scale morphology, *Icarus*, 210, pp. 545–565, doi:10.1016/j.icarus.2010.07.021

- Millour, E., F. Forget, A. Spiga, T. Navarro, J.-B. Madeleine, A. Pottier, L. Montabone, L. Kerber, A. Colaitis, F. Lefèvre, F. Montmessin, J.-Y. Chaufray, M. A. López-Valverde, G. González-Galindo, S. R. Lewis, P. L. Read, M.-C. Desjean, J.-P. Huot, MCD/GCM Development Team (2014) A new Mars Climate Database v. 5.1, The Fifth International Workshop on the Mars Atmosphere: Modelling and Observation, January 13-16 2014, Oxford, U.K., id: 1301
- Montmessin, F., B. Gondet, J.-P. Bibring, Y. Langevin, P. Drossart, F. Forget, T. Fouchet (2007) Hyperspectral imaging of convective CO₂ ice clouds in the equatorial mesosphere of Mars, *J. Geophys. Res.*, 112, E11S90, doi: 10.1029/2007JE002944
- Moudden, Y. and J.M. Forbes (2008) Effects of vertically propagating thermal tides on the mean structure and dynamics of Mars' lower thermosphere, *Geophys. Res. Lett.*, 35, L23805, doi: 10.1029/2008GL036086
- Moudden, Y. and J.M. Forbes (2010) A new interpretation of Mars aerobraking variability: Planetary wave-tide interactions, *J. Geophys. Res.*, E09005, doi: 10.1029/2009JE003542
- Moudden, Y. and J.M. Forbes (2011) Simulated planetary wave-tide interactions in the atmosphere of Mars, *J. Geophys. Res.*, 116, E01004, doi: 10.1029/2010JE003698
- Moudden, Y. and J. M. Forbes (2014) Insight into the seasonal asymmetry of nonmigrating tides on Mars, *Geophys. Res. Lett.*, 41, pp. 2631–2636, doi: 10.1002/2014GL059535
- Nier, A.O. and M.B. McElroy (1977) Composition and structure of Mars' upper atmosphere: Results from the Neutral Mass Spectrometers on Viking 1 and 2, *J. Geophys. Res.*, 82, 28, pp. 4341-4349, doi: 10.1029/JS082i028p04341
- Sato, T.M., H. Fujiwara, Y.O Takahashi, Y. Kasaba, V. Formisano, M. Giuranna, D. Grassi (2011) Tidal variations in the Martian lower atmosphere inferred from Mars Express Planetary Fourier Spectrometer temperature data, *Geophys. Res. Lett.*, 38, L24205, doi: 10.1029/2011GL050348
- Schoenenberger, M., F.M. Cheatwood, P.N. Desai (2005) Static Aerodynamics of the Mars Exploration Rover Entry Capsule, 43rd AIAA Aerospace Sciences Meeting & Exhibit, AIAA-2005-0056, 10-13 January 2005, Reno, NV, USA
- Schoenenberger, M., J. van Norman, C. Karlgaard, P. Kutty, D. Way (2014) Assessment of the Reconstructed Aerodynamics of the Mars Science Laboratory entry vehicle, *J. Spacecraft and Rockets*, 51, No. 4, doi: 10.2514/1.A32794
- Scholten, F., H. Hoffmann, A. Määttänen, F. Montmessin, B. Gondet, E. Hauber (2010) Concatenation of HRSC colour and OMEGA data for the determination and 3D-parameterization of high-altitude CO₂ clouds in the Martian atmosphere, *Planet. Space Science*, 58, pp. 1207–1214, doi: 10.1016/j.pss.2010.04.015

- Spiga, A., F. González-Galindo, M.-Á. López-Valverde, F. Forget (2012) Gravity waves, cold pockets and CO₂ clouds in the Martian mesosphere, *Geophys. Res. Lett.*, 39, L02201, doi: 10.1029/2011GL050343
- Tillman, J.E. (1988) Mars global atmospheric oscillations – Annually synchronized, transient normal mode oscillations and the triggering of global dust storms, *J. Geophys. Res.*, 93, pp. 9433-9451, doi: 10.1029/JD093iD08p09433
- Way, D.W., J.L. Davis, J.D. Shidner (2013) Assessment of the Mars Science Laboratory Entry, Descent, and Landing Simulation, 23rd AAS/AIAA Space Flight Mechanics Meeting, AAS 13-420, February 10-14, 2013, Kauai, Hawaii, USA
- Wilson, R.J. (2002) Evidence for nonmigrating thermal tides in the Mars upper atmosphere from the Mars Global Surveyor Accelerometer Experiment, *Geophys. Res. Lett.*, 29, doi: 10.1029/2001GL013975
- Wilson, R.J. and K. Hamilton (1996) Comprehensive model simulation of thermal tides in the Martian atmosphere, *J. Atmos. Sci.*, 53, pp. 1290-1326, doi: [http://dx.doi.org/10.1175/1520-0469\(1996\)053<1290:CMSOTT>2.0.CO;2](http://dx.doi.org/10.1175/1520-0469(1996)053<1290:CMSOTT>2.0.CO;2)
- Withers, P. (2006), Mars Global Surveyor and Mars Odyssey Accelerometer observations of the Martian upper atmosphere during aerobraking, *Geophys. Res. Lett.*, 33, L02201, doi: 10.1029/2005GL024447
- Withers, P. (2013) A smoothing technique for improving atmospheric reconstruction for planetary entry probes, *Planet. Space Sci.*, 79-80, doi: 10.1016/j.pss.2013.01.011
- Withers, P., S.W. Bougher, .G M. Keating (2003) The effects of topographically-controlled thermal tides in the martian upper atmosphere as seen by the MGS accelerometer, *Icarus*, 164, pp. 14-32, doi: 10.1016/S0019-1035(03)00135-0
- Wither, P., M.C. Towner, B. Hathi, J.C. Zarnecki (2003) Analysis of entry accelerometer data: A case study of Mars Pathfinder, *Planet. Space Sci.*, 51, pp. 541-561, doi: 10.1016/S0032-0633(03)00077-1
- Withers, P. and M.D. Smith (2006) Atmospheric entry profiles from the Mars Exploration Rovers Spirit and Opportunity, *Icarus*, 185, pp. 133-142, doi: 10.1016/j.icarus.2006.06.013
- Withers, P. and D.C. Catling (2010) Production of Reduced Data Records for the Phoenix Atmospheric Structure Experiment, NASA Planetary Data System, PHX-MASE-5-EDL-RDR-V1. 0
- Withers, P., L. Pratt, J.-L. Bertaux, F. Montmessin (2011) Observations of thermal tides in the middle atmosphere of Mars by the SPICAM instrument, *J. Geophys. Res.*, 116, E11005, doi: 10.1029/2011JE003847
- Zurek, R.W. (1976) Diurnal tide in the martian atmosphere, *J. Atmos. Sci.*, 33, pp. 321-337, doi: [http://dx.doi.org/10.1175/1520-0469\(1976\)033<0321:DTITMA>2.0.CO;2](http://dx.doi.org/10.1175/1520-0469(1976)033<0321:DTITMA>2.0.CO;2)

Zurek, R.W. (1980) Surface Pressure Response to Elevated Tidal Heating Sources: Comparison of Earth and Mars, *J. Atm. Sci.*, 37, pp. 1132-1136, doi: [http://dx.doi.org/10.1175/1520-0469\(1980\)037<1132:SPRTET>2.0.CO;2](http://dx.doi.org/10.1175/1520-0469(1980)037<1132:SPRTET>2.0.CO;2)

Zurek, R.W. and Leovy, C.B. (1981) Thermal tides in the dusty martian atmosphere: A verification of theory, *Science*, 213, pp. 437-439, doi: [10.1126/science.213.4506.437](https://doi.org/10.1126/science.213.4506.437)

Zurek, R.W. (1986) Atmospheric tidal forcing of the zonal-mean circulation – The Martian dusty atmosphere, *J. Atmos. Sci.*, 43, pp. 652-670, doi: [http://dx.doi.org/10.1175/1520-0469\(1986\)043<0652:ATFOTZ>2.0.CO;2](http://dx.doi.org/10.1175/1520-0469(1986)043<0652:ATFOTZ>2.0.CO;2)

Zurek, R.W. et al. (1992) Dynamics of the atmosphere of Mars, in *Mars*, ed. Kieffer et al., University of Arizona Press, pp. 835-933, ISBN: 0-8165-1257-4

7. FIGURES

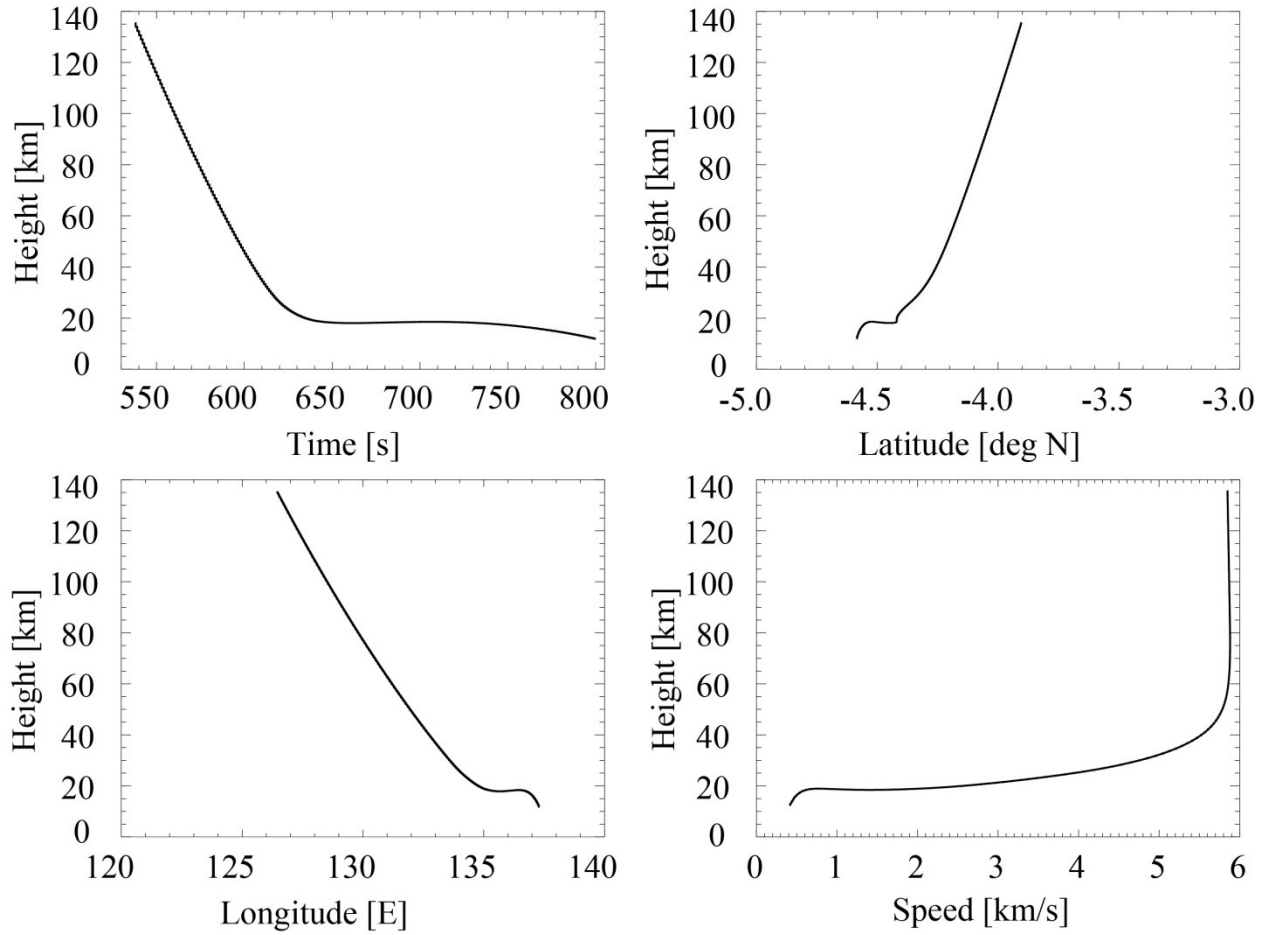


Figure 1: MSL entry trajectory (time, latitude and longitude) and spacecraft speed as a function of height above the landing site from atmospheric entry to parachute deployment. The horizontal flight period is clearly visible just below 20 km height.

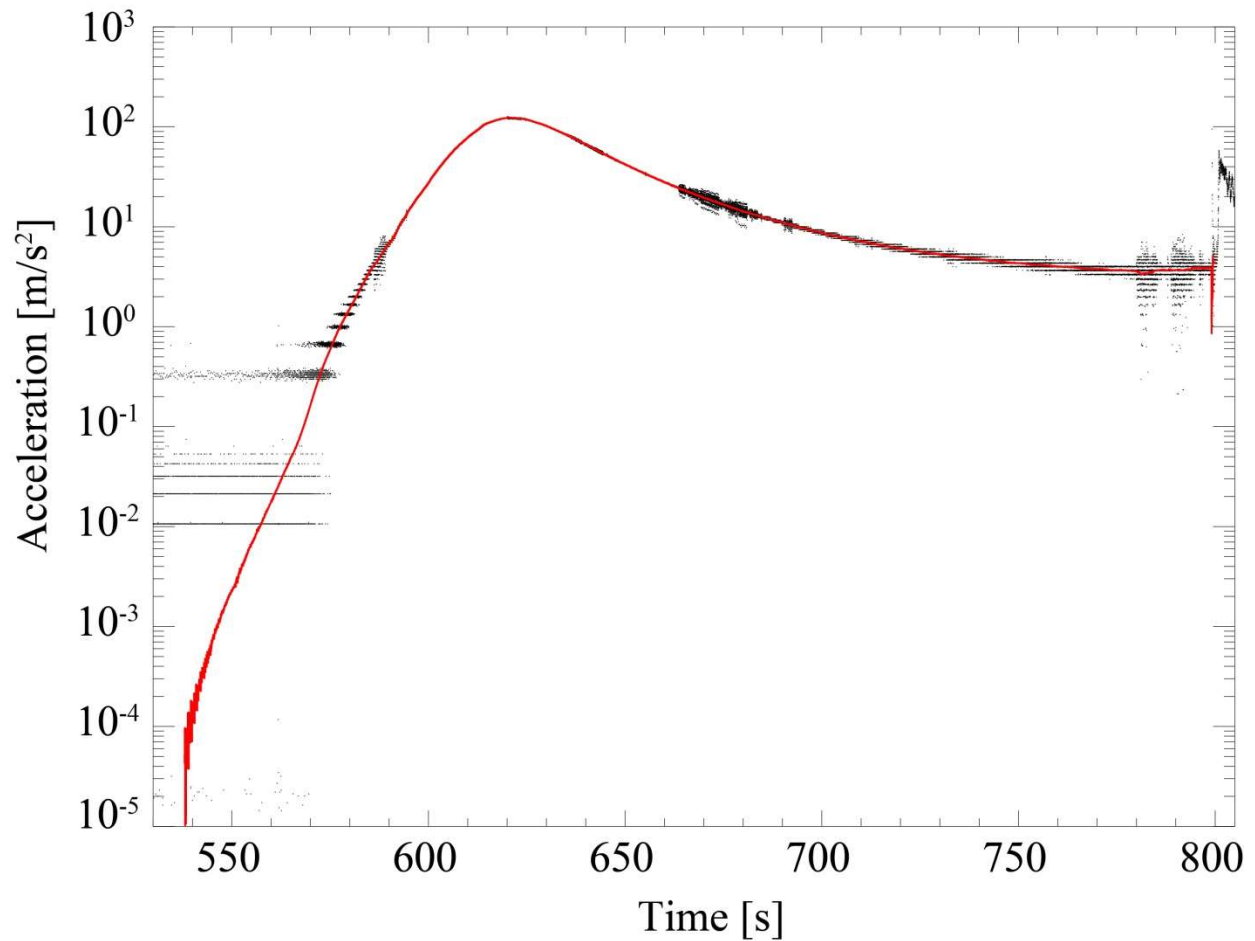


Figure 2: Measured axial accelerations (black points) and smoothed axial accelerations (red line) as a function of time for the MSL EDL. Instrument digitization is visible in the measured accelerations prior to 570 s, and data noise shows up after 650 s due to bank reversals and spacecraft heading alignment. Events evident in the data are peak deceleration at 620 s, ballast mass ejections at 780 s and parachute deployment at 799 s. Atmospheric entry occurred at $t = 540$ s at a radius of 3522.2 km (Karlgaard et al. 2014).

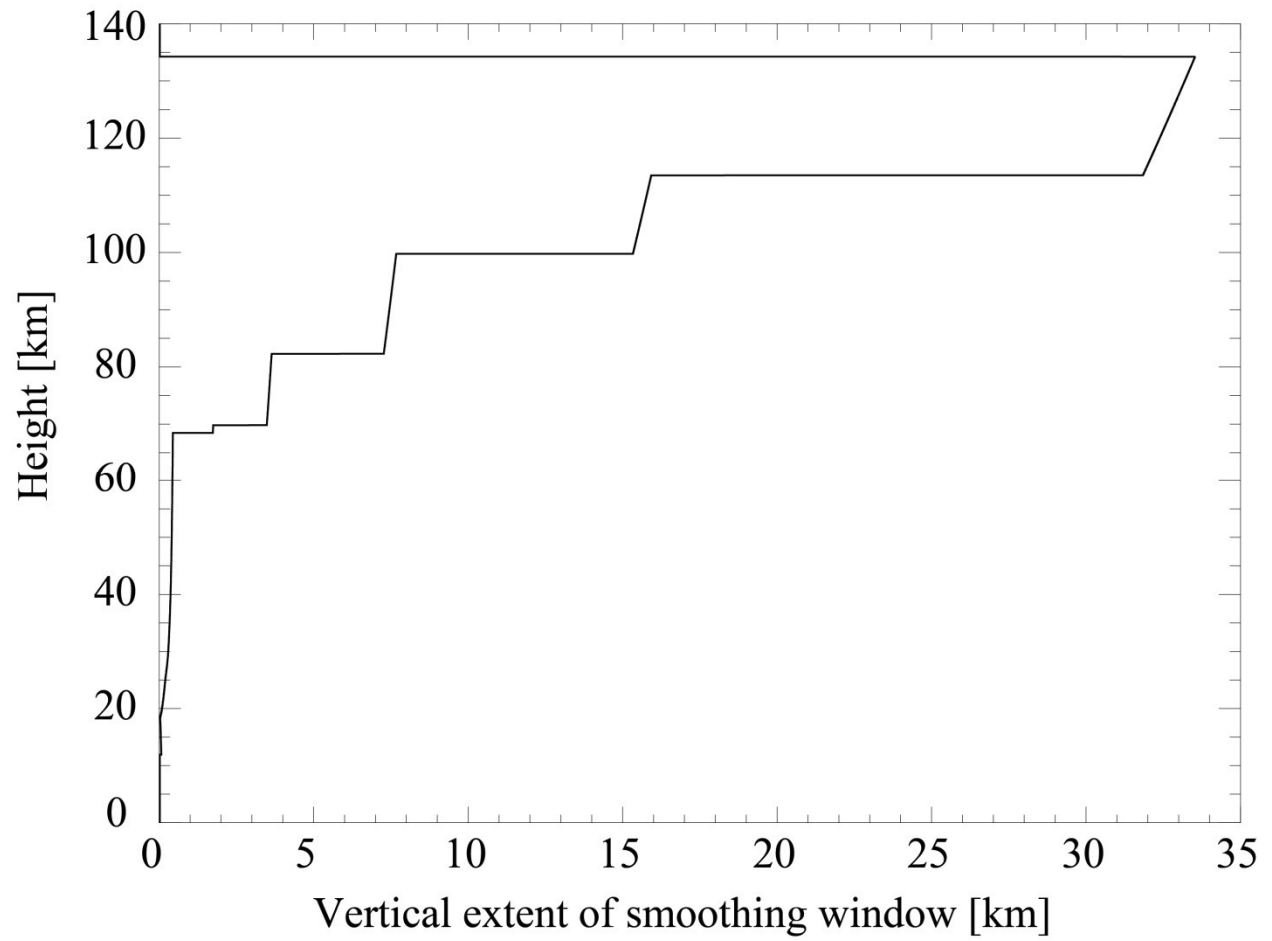


Figure 3: Vertical resolution, or vertical extent, of smoothing window as a function of height above the landing site.

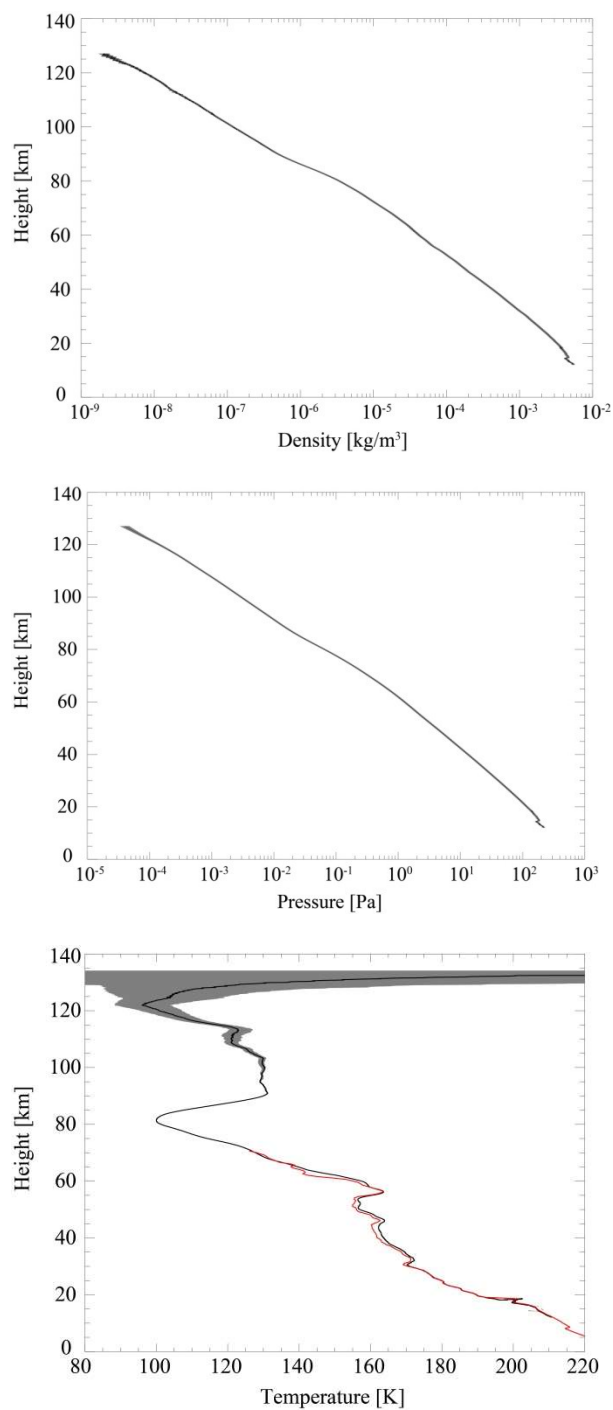


Figure 4: The reconstructed MSL density, pressure and temperature profiles as a function of height above the landing site with one sigma error envelopes in gray. The reconstructed JPL temperature profile from Chen et al. (2014) is shown in red in bottom panel.

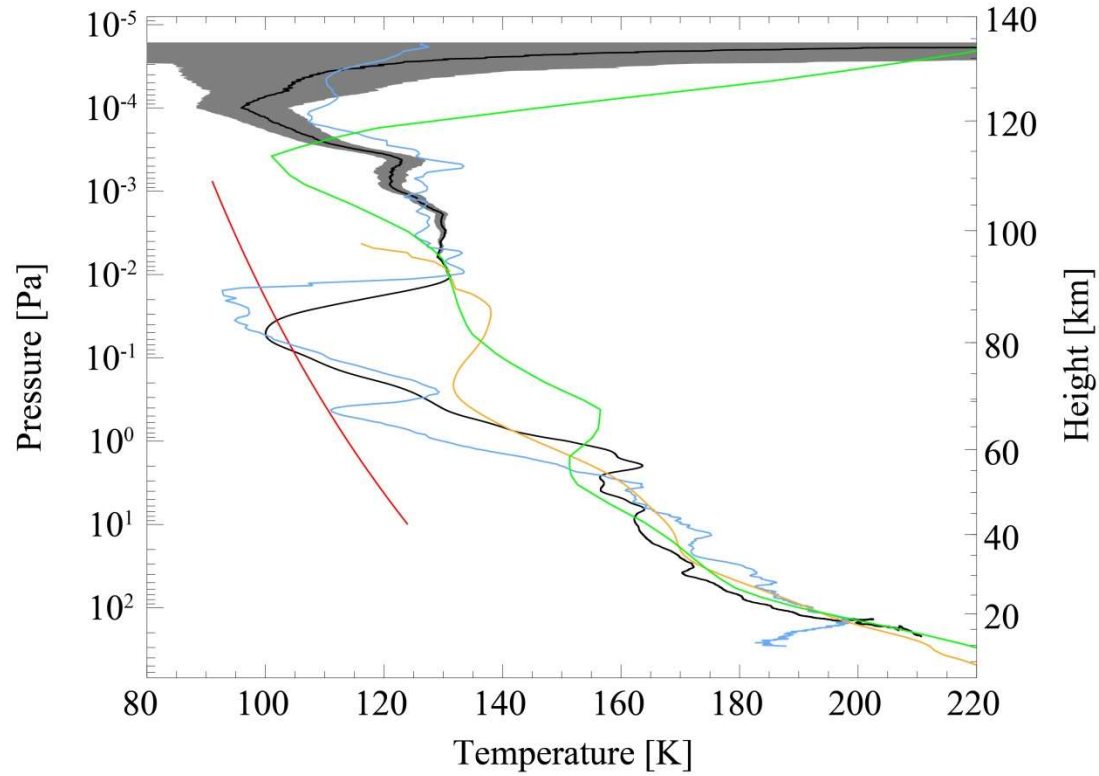


Figure 5: The reconstructed MSL temperature profile (black) as function of pressure with one sigma error envelope. Overlain are the CO₂ condensation curve (red), the Mars Pathfinder EDL temperature profile (blue), the Mars Climate Database (MCD) temperature profile for the time and position of the MSL landing (green) and the average temperature profile from MCS from the week leading up to the landing of MSL (orange).

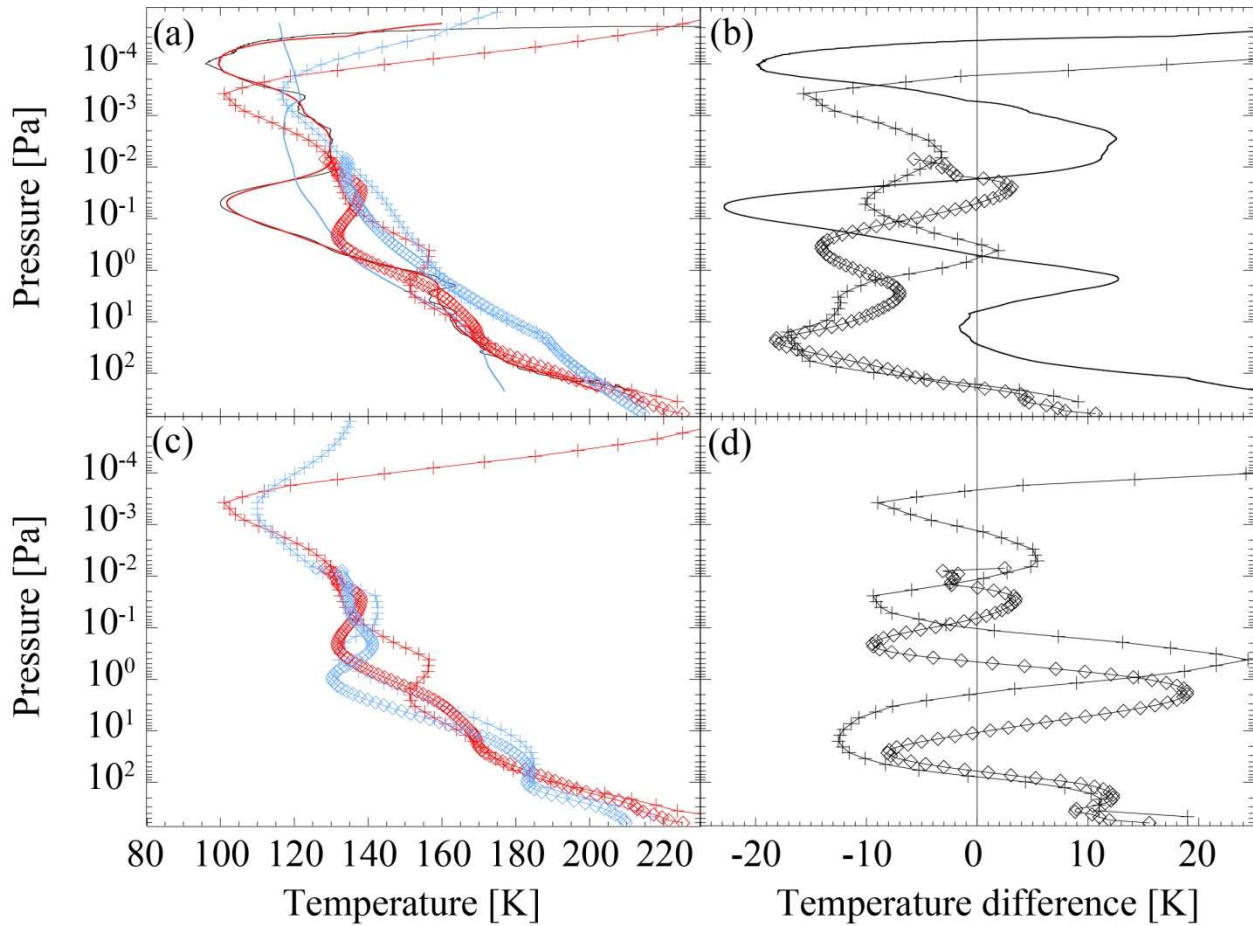


Figure 6: (a) Daytime (red) and 3 scale height averaged (blue) temperature profiles for MSL (solid lines), MCS (diamonds) and MCD (crosses). The black line is the original MSL temperature profile (b) Temperature differences between daytime and 3 scale height averaged temperature profiles for MSL, MCS and MCD (c) Daytime (red) and nighttime (blue) temperature profiles for MCS and MCD (d) As panel (b) but calculated from temperature profiles in panel (c).

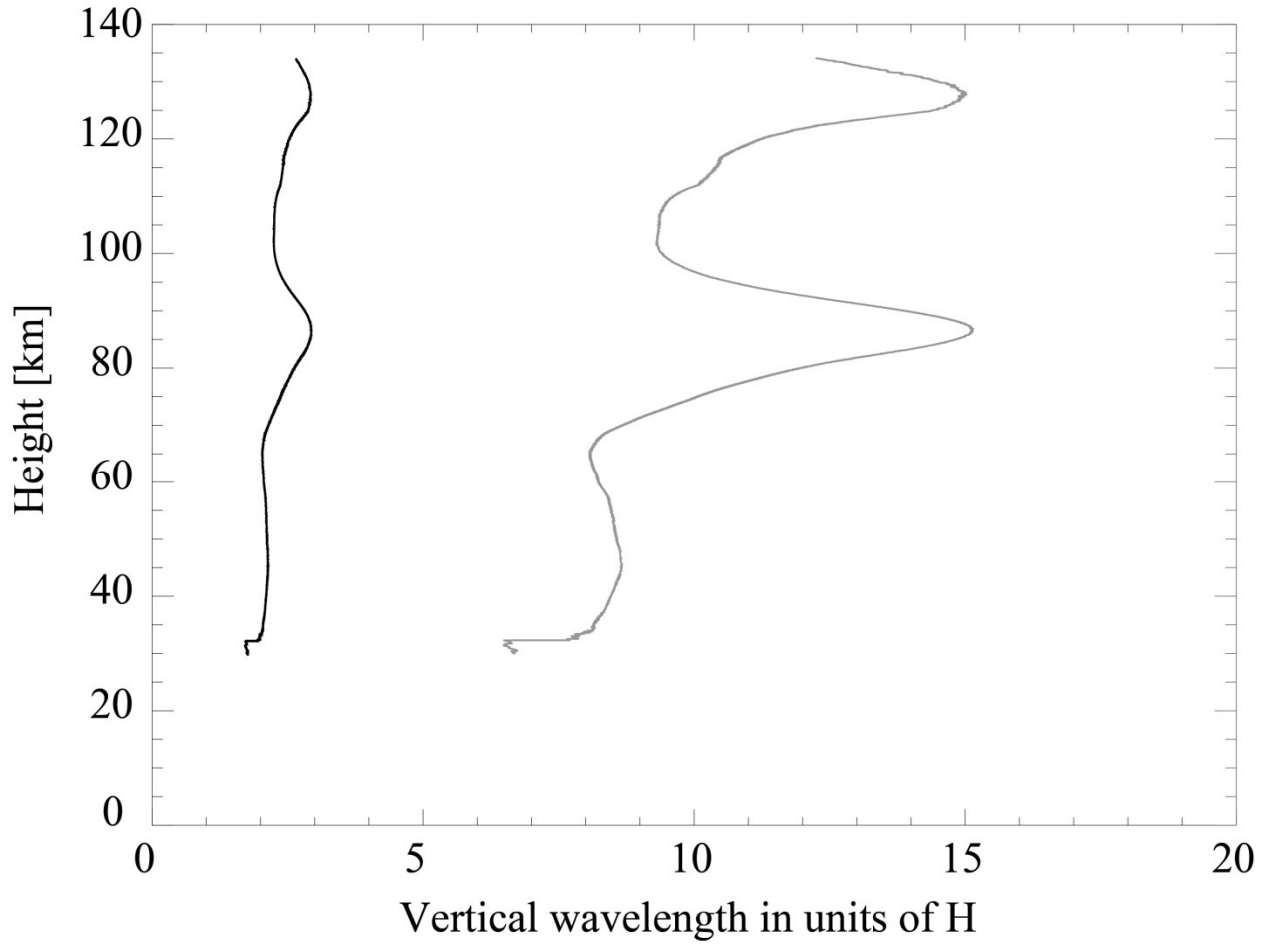


Figure 7: Vertical wavelengths in units of scale height as a function of height above the landing site, calculated from the idealized wave theory for the diurnal migrating tide (black line) and semidiurnal migrating tide (grey line).

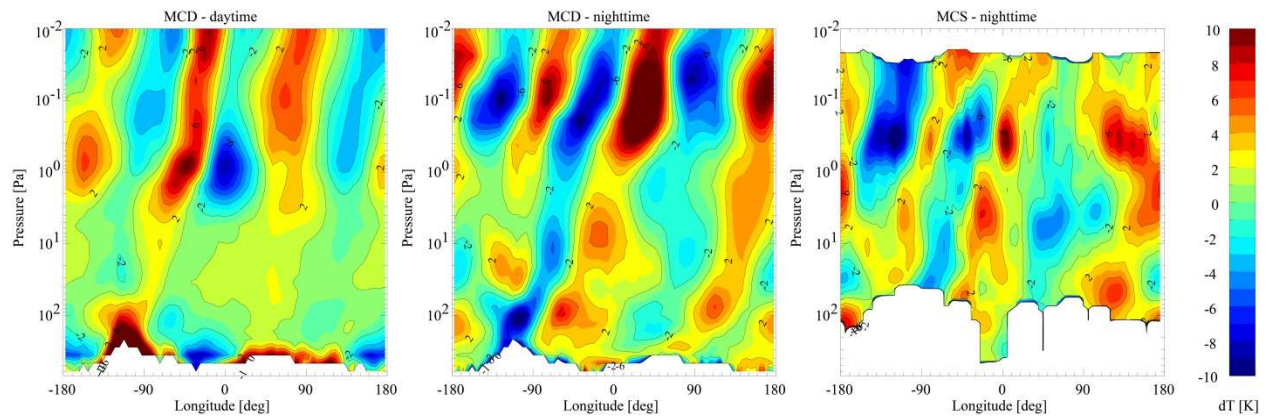


Figure 8: Contour plots of the difference between average temperature profiles and the zonal mean subtracted as a function of pressure. From left to right: MCD output for MSL time of landing, MCD output for 12 hours prior to MSL time of landing, and MCS profiles from 02-04 LTST. For the MCD output, temperature profiles were obtained for every 5° of longitude and every 2.5° of latitude between 12.1°S and 2.9°N . The same latitude interval and a 5° longitude binning were used to compile average MCS temperature profiles.